arXiv:2104.02058v1 [eess.SP] 1 Apr 2021

Neurological Status Classification Using Convolutional Neural Network

Mehrad Jaloli * **Divya Choudhary** ** **Marzia Cescon** *

* *Dept. of Mechanical Engineering, University of Houston, Houston, TX United States 77004*
** *Dept. of Biochemistry, University of Oxford, South Parks Road, Oxford, OX1 3QU, UK*

(Corresponding e-mail: mcescon2@uh.edu)

Abstract:
In this study we show that a Convolutional Neural Network (CNN) model is able to accurately discriminate between 4 different phases of neurological status in a non-Electroencephalogram (EEG) dataset recorded in an experiment in which subjects are exposed to physical, cognitive and emotional stress. We demonstrate that the proposed model is able to obtain 99.99% Area Under the Curve (AUC) of Receiver Operation characteristic (ROC) and 99.82% classification accuracy on the test dataset. Furthermore, for comparison, we show that our models outperforms traditional classification methods such as SVM, and RF. Finally, we show the advantage of CNN models, in comparison to other methods, in robustness to noise by 97.46% accuracy on a noisy dataset.

Keywords: Assistive devices; Cognitive control; Potential impact of automation and open problems; Deep neural network; Physiological signal processing; Neurological status assessment

1. INTRODUCTION

Physiological changes in the human body are accompanied by, or are a results of, changes in neurological status. In conditions such as diabets [Farrell et al. (2004)] or seizures [Mueller et al. (1979)], it has been shown that a surge in stress levels was linked to a deterioration in patients health condition. Recent improvements at the interface of healthcare and technology allowed to track neurological changes during arousal/stress and infer the subject's underlying neurological state at each time instant. However, most of those studies have used neurological datasets like electroencephalogram (EEG) [Al-Shargie et al. (2015)] or functional magnetic resonance imaging (fMRI) [Dopfel and Zhang (2018)], which mostly have invasive, uncomfortable and time-consuming data collection protocols.

With the advent of non-invasive sensors built-in devices and the rapid growth in the adoption of wearable devices, it is now possible to collect different types of physiological signals that can be leveraged to monitor internal physiological changes. Some of this signals that may be useful in studying the neurological status are electrodermal activity (EDA), heart rate (HR), accelerometer (ACC), skin temperature (Temp) and respiratory rate [Cogan et al. (2014)].

In particular, previous studies on EDA and HR have shown that features extracted in both frequency and time domain are relevant for neurological status analysis. Posada-Quintero and coworkers showed in [Posada-Quintero et al. (2018)] how the EDA signal dynamics shift in various ranges of frequency and Ghiasi et al. (2020) showed how heart rate along with EDA signal contributes in detecting the arousal levels. Such studies have inspired researchers to build more analytically powerful tools and methods to accurately predict the intensity and type of the stress and also qualitatively analyse its correlation with physiological changes and external stimuli.

Against this background, our goal is to develop and verify a method which is able to discriminate between different stages of neurological status and arousal in a non-EEG dataset. The outline of the paper is as follows. Section 2 introduces some background on deep neural networks; in section 3 the dataset is presented followed by the explanation of the preprocessing steps. Sections 4 and 5 explain the results and conclusions, respectively;

2. DEEP NEURAL NETWORK

Artificial neural networks (ANN) are categorized as a type of machine learning algorithms inspired by the human brain, consisting of a stack of neurons, called layers, such that the neurons within the same layer are not connected to each other. Deep neural networks, in particular are types of ANNs with multiple layers connecting input and output layers, called hidden layers [LeCun et al. (2015a)]. The input layer, receives the input data, the hidden layers are where the input is processed and the output layer provides the output of the model.

[1] This research was supported by the University of Houston through a start-up grant.

2.1 Convolutional Neural Network (CNN)

CNN is a well-known deep learning architecture that has demonstrated an excellent performance in computer vision and image classification problems [Karpathy et al. (2014)]. It has been proven to have many advantages over other machine learning algorithms like robustness to noise, automatic feature extraction, weight sharing characteristic, being suitable for working with incomplete patterns and flexible structures which makes them a compatible and proper tool for facing with different size of datasets and complicated problems.

A CNN model is generally composed of two parts: 1) feature extraction, which includes several convolution layers followed by pooling layers and activation functions and 2) classification part that is consisted of fully connected layers, structured the same as an ANN, which exploits the extracted features from the first part and performs the classification task.

Generally, there are three well-known CNN structures, all can be used in classification problems: 1 dimensional CNN (1D CNN), 2 dimensional CNN (2D CNN) and 3 dimensional CNN (3D CNN). 1D CNN is able to derive features from fixed-length slices of a dataset, by sliding 1 dimensional convolution filters all along each slice (window) such that the width of the filter is equal to the width of the dataset. Such properties makes 1D CNN a very powerful and fast method in identifying simple patterns within a data which can be used for more complex patterns in higher layers of the model.

2D and 3D CNNs, have the same aforementioned characteristics, while the difference is in the dimensionality of the input data and convolutional kernels. In 2D CNN , 2D filters slide in both width and height dimensions of the data segment. It is mostly applied on image datasets, where the spatial information of the features is of interest in addition to features by its own [LeCun et al. (2015b)]. However, 3D CNN in which 3D kernels move through 3 dimensions of the data, height, width and depth, is mostly used in video datasets, due to the capability of extracting features from both the spatial and the temporal dimension of the segments of the dataset [Ji et al. (2012)].

Fig 1 shows a sample CNN model, where the input is an image of size $H_I \times W_I \times D_I$, with H_I, W_I and D_I being height, width and depth, or number of color channels, of the input image, respectively. The image is turned to a tensor of raw pixels, to be able to fed and analyzed by a CNN model.

In a 2D CNN, filters of size H_f, W_f slide all over the tensors in a separate manner and result a deeper tensor called feature map. In cases that we have no padding , the size of the output of each convolution layer with stride 1 is $H_{conv} \times W_{conv} \times D_f$ such that:

$$H_{conv} = H_I - H_f + 1 \tag{1}$$

$$W_{conv} = W_I - W_f + 1 \tag{2}$$

and D_f is the number of filters of a convolution layer. W_I, W_{conv}, H_I, H_{conv} are the width and height of the convolution layer input and output, respectively. H_f and W_f are height and width of the filter. Note that in 1D CNN, the width of the filter, W_f, is equal to the width of data segments, W_I. Afterward, to apply a nonlinear transformation, the output of the convolution layer is sent to an activation function. Some common activation functions are rectified linear unit (RELU), tangent hyperbolic (TanH), exponential Linear units (ELU), softmax. Table 1 lists the corresponding mathematical expressions. Note that in ELU equation, $a \geq 0$ is a hyper-parameter that needs to be tuned.

Table 1. Activation Functions

Activation Function	Equation
RELU	$f(x) = \begin{cases} x \ for \ x > 0 \\ 0 \ for \ x < 0 \end{cases}$
TanH	$f(x) = \frac{e^x - e^{-x}}{e^x + e^{-x}}$
ELU	$f(a,x) = \begin{cases} x & for \ x \geq 0 \\ a(e^x - 1) & for \ x < 0 \end{cases}$
Softmax	$f(x) = \frac{1}{1+e^{-x}}$

In order to reduce the amount of parameters and computational load and avoid over-fitting, feature maps are sub-sampled into lower-dimensions using pooling layers. Two of the most common pooling layers are Maxpooling and Average pooling. By applying max/average pooling function of size H_p , W_p, the max/average of each region of size (H_p, W_p) is calculated and outputs a subsampled feature map with size:

$$W_{p\ out} = (W_{conv} - W_p)/s + 1 \tag{3}$$

$$H_{p\ out} = (H_{conv} - H_p)/s + 1 \tag{4}$$

Where s is the stride or step size and $H_{p\ out} \times W_{p\ out} \times D_{conv}$ is the size of the output of pooling layer, respectively. Generally, we may have more than 1 convolution and pooling layer, depending on the complexity of the problem and amount of available dataset.

The output of the feature extraction part, is fed to the fully-connected layers, where it is passed through hidden layer's activation functions and finally a softmax activation function at the output of the last fully-connected layer, such that the class to which the input of the model belongs to is determined. Note that the number of neurons at the output layer is equal to the number of classes. Equation 5 shows how a class is detected at the output layer.

$$\arg \max_{0<k<c} P_k(x) = f(X_i) \tag{5}$$

where, c is the number of classes, $P_c(x)$ is the confidence score for predicting class k. X_i is the i^{th} sample (input)

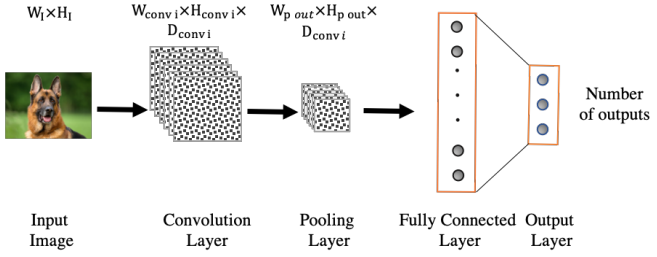


Fig. 1. Illustration of the CNN architecture. Convolutional layer, pooling layer and fully connected layer are the core CNN operation and output layer is final output.

and $f(.)$ is the softmax activation function. The class with the highest confidence score is the predicted class.

Having such various characteristics, CNN application has been extended to more challenging domains like time series prediction and classification.

2.2 Time series classification (TSC)

Combined with time series, deep learning frameworks can be used as a predictive tool, e.g. predicting neurological disorders like epileptic seizure[Cogan et al. (2014)], or neurological sicknesses like cybersickness [Islam et al. (2020)], diagnostic method, like cardiovascular disorder detection [Rajpurkar et al. (2017)], or even therapeutic [Liu et al. (2020)] approaches in healthcare problems.

Time series classification (TSC) is referred to the task of training a classifier on a set of time sequences, X, with the corresponding labels, Y, such that the trained classifier is able to predict the labels of a previously unseen test dataset [Ebadi et al. (2019), He et al. (2015)].

Previous works have used different methods for TSC using distance measures, namely: euclidean distance (ED), dynamic time warping (DTW) [Ratanamahatana and Keogh (2005)e] and edit distance with real penalty (ERP) [Chen and Ng (2004)]. Further, Keogh and Kasetty (2003) claimed that machine learning algorithms significantly outperform those traditional and empirical methods.

Kampouraki et al. (2008) applied a support vector machine (SVM) method for heartbeat classification. Chaovalitwongse et al. (2007) used K-nearest neighbors (KNN) method to classify the brain abnormal activity. Moreover, random forest (RF), a machine learning algorithm that fits a number of decision tree classifiers on various sub-samples of the dataset, has been proposed to be a promising tool in TSC problems [Deng et al. (2013)]. Nonetheless, in order to be an accurate tool, all aforementioned machine learning methods need a feature extraction process before feeding the data into the model.

Due to having the ability of automatic feature extraction, CNN can solve this problem. Moreover, Zeiler and Fergus (2014) has shown that 1D and 2D CNN could be a powerful in analyzing signals, where we have multi-modal time series.

3. MATERIALS AND METHODS

3.1 Dataset

We used a publicly available data set for assessment of Neurological Status [Goldberger et al. (2000)], comprising accelerometer in 3 dimensions (ACC), electrodermal activity (EDA) and body temperature (T) collected with a sample frequency of 8 [Hz]; heart rate (HR) and an estimate of the amount of oxygen in the blood calculated by oxygen saturation (SpO2) sampled at 1 [Hz]. Data was collected with wrist-worn sensors from 20 college students (6F/14M, age = 26.05 ±3.8 yrs) undergoing various experiments with the purpose of probing a subject's response to different types of stress.

The experimental protocol is shown in Fig 2

Five minutes were recorded for each of the following stages: relaxation, physical activity, cognitive stress and emotional stress. Relaxation is considered as the baseline, while physical activity is broken into three parts with different intensities: standing for one minute, walking for two minutes and finally jogging for two minutes. After another five minutes relaxation, the individuals experience a cognitive stress stimulation consisting in counting backward a list of numbers for 3 minutes and then take the Stroop test for 2 minutes which is reading the names of colors written in different color ink and saying what color the ink is. Finally, after another five minutes relaxation, subjects are shown a a horror movie for five minutes to be emotionally stimulated.

In order to avoid redundancy, among all the relaxation phases, we only included the first one into our computations. Moreover, the first 40 seconds of the cognitive phase, during which the subjects received explanations on the clinical protocol regarding the experiments, were considered as emotional phase, given that subjects showed patterns similar to the emotional patterns.

We are going to apply a CNN classifier to discriminate the dataset into 4 phases, i.e Relaxation, Physical activity, Cognitive stress, Emotional stress.

3.2 Data Preprocessing

The data for each individual was separated into four phases: relaxation, physical activity, cognitive stress and emotional stress. Then the data for all subjects were concatenated along time axis.

To have the aggregated information of all three dimensions in one variable (time series), the magnitude of the 3D accelerometer signal was computed as:

$$ACC = \sqrt{\sum_{i=0}^{l} x_i^2 + \sum_{i=0}^{l} y_i^2 + \sum_{i=0}^{l} z_i^2} \tag{6}$$

Where l represents the length of signal.

It is a well known fact that EDA can be modeled as a sum of three terms: the phasic and tonic components plus an additive noise (see Eq. 7) [Greco et al. (2015)].

The phasic component is an impulse-shaped signal describing the sudden changes in EDA signal, however, tonic is a smooth-shaped sequence corresponding with the slow changes in EDA.

$$e_k = p_k + t_k + \epsilon_k \tag{7}$$

where k is the time index, e_k, p_k and t_k represent the eda, phasic and tonic component, respectively, and ϵ_k is a an independent and identically distributed (iid) signal with mean zero and variance 1 (Gaussian Random Variable),

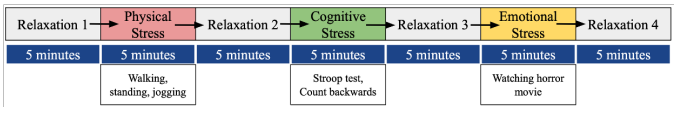


Fig. 2. Experiment design for data collection. Relaxation is used for helping the subjects get to the baseline after each stimulation phase.

representing the additive noise term. Note that all terms, e_k, p_k , t_k and ϵ_k are the same length column vectors.

In addition to these three variables, HR and SpO2 variables are also taken into account for our computations. Since we are dealing with a multi-variate dataset, to solve the problem of having various distribution for each variable, we use Z-score method [Kellaway (1969)] for each of them separately:

$$Z = \frac{X_i - \mu_i}{\sigma_i} \tag{8}$$

where X_i is the variable, μ_i and σ_i are the associated mean and the standard deviation of the variable, respectively, and $i = 1, ..., , 25$ is the number of variables, which in our case is 25.

Moreover, we took the first, second and third derivative of each variable in time domain separately, and stacked the resulted variables below the time-domain components.

Furthermore, prompted by a previous study of our group [Choudhary et al. (2020)], showing that there are relations between changes in neurological status and frequency components of simultaneously recorded physiological signals, we computed the frequency component, the absolute magnitude of the short time Fourier transform (STFT) (Eq. 9), for each time series to capture the signal's frequency content over time. Then we stacked the resulted 5 variables in frequency domain, below the time domain variables.

$$X(\tau, \omega) = \int_{-\infty}^{\infty} x(t) w(t - \tau) e^{-i\omega t} dt \tag{9}$$

where $w(\tau)$ is the window function, $x(t)$ is the signal in time domain and $X(\tau, \omega)$ is the Fourier transform representing the magnitude and phase of $x(t)$ over time and frequency. τ and ω are time and frequency index, respectively. It should be mentioned that we only take magnitude of $X(\tau, \omega)$ as the frequency component of each variable. As a result, we acquired a 25 variable dataset, consisting of initial time domain components, frequency components and first, second and third derivatives of time domain variables.

Finally, to make the data ready for being fed into the CNN model, we used sliding windows of width 25 and length 30, equal to the number of variables, with 50% overlap and moved it all along the dataset to create samples of size 25 $\times$ 30.

To compare the effect of each sets of variables, we created datasets with different number of variables such that: dataset one only includes the raw signals in time domain, dataset two includes time and frequency components. The third, fourth and fifth datasets includes components of time domain along with the first, second and third derivatives, respectively. Dataset six includes time, frequency and first derivatives.The seventh one consists of the time, frequency, and second derivatives and finally the eighth one comprises all 25 variables.

4. RESULTS

4.1 1D CNN

After training the model with all parameters in Table 1 the best results were acquired by using ELU with $a = 1$ as the activation function of the convolution layers, since it diminishes the vanishing gradient effect, and TanH for hidden layers of the neural network. Moreover, Root Mean Square Propagation (RMSprop) with learning rate of 0.001 and the Categorical Cross Entropy was selected as the optimization algorithm and the loss function, respectively.

Since we had 25 variables, to know the effect of each set of them on our classification results, i.e, dataset one to eight, we trained the 1D-CNN for all datasets separately.

To make sure that the training, validation and test datasets are representative of the overall distribution of the dataset, we apply shuffling such that all training, validation and test datasets may include information from all subjects.

Then, We split the data into 70% for training, 10% for validation during training and 20% for the test dataset. Table 2 shows the training results of the 1D CNN for 100 epochs and batch size of 32, for different datasets. Accuracy, area under the curve of the receiver operation characteristic (AUC-ROC) and area under the recall-precision curve (AUC-RP) are used as the evaluation metrics to compare the results. We can see that using all 25 variables can significantly improve the results, hence we will use the dataset number eight.

Table 2. Results of training 1D CNN with different combinations of components

Dataset	Accuracy (%)	AUC-ROC	AUC-RP
One	95.14	0.968	0.979
Two	97.0	0.978	0.984
Three	96.45	0.975	0.983
Four	95.31	0.969	0.980
Five	95.2	0.998	0.979
Six	97.36	0.978	0.983
Seven	98.05	0.985	0.987
Eight	**99.82**	**0.999**	**0.998**

Table 3 demonstrates the performance of the 1D CNN model evaluated with other metrics, namely: precision, recall and F1-score of each classes as well as the total clas-

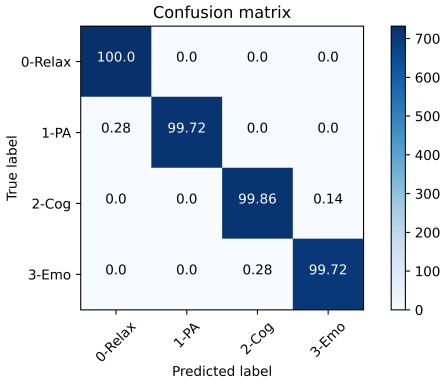


Fig. 3. Confusion matrix for 1D CNN model (%)

sification accuracy. Moreover, figure 3 shows the confusion matrix.

Table 3. Evaluation results of the 1D CNN model

Class	Precision (%)	Recall (%)	F1-Score (%)
Relaxation	99.72	100.00	99.85
Physical Activity	99.72	99.72	99.72
Cognitive Stress	99.72	99.86	99.78
Emotional Stress	99.85	99.72	99.78
	Accuracy	**99.82**%	

4.2 2-Dimensional CNN

We also implemented a 2D CNN using the same hyper parameters and split size as we used for 1D CNN. Results of training after 150 epochs, using early stopping point and with batch size of 32 is shown in Table 4. Moreover, figure 4 shows the confusion matrix of 2D CNN for classifying the whole dataset of size 25 variables into the 4 neural stages.

4.3 Comparison with SVM and RF

To better evaluate the benefits of CNNs in the neurological status classification task at hand, we trained a multi-class SVM and a RF model and subsequently compared the results obtained to those of CNNs.

Since for training these models we need to apply a feature extraction method prior to training the model, the following statistical features were extracted from each of the windows (samples) of the dataset: *mean, maximum, minimum, range* (the amount of changes for each variable from beginning to the end of each window) and the *first derivative*.

For training a multi-class SVM, after creating the parameter grid based on the results of random search, the best parameters were obtained using Grid Search method such that, the regularization parameter, C, was set to 100, gamma value 0.001 and the Radial Basis Kernel (RBF) was selected.

Moreover, the same features were used for training a RF model with complexity parameter of zero, 150 random state, number of estimator of 130 and the gini criterion.

As Table 5 shows the classification accuracy and F-1 score resulted from each method, we can see that 1D and 2D

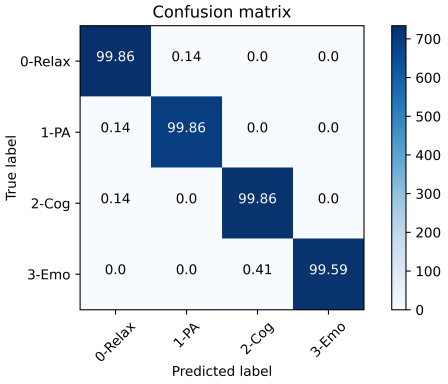


Fig. 4. Confusion matrix for 2D CNN model (%))

Table 4. Evaluation results of the 2D CNN model

Class	Precision (%)	Recall (%)	F1-Score (%)
Relaxation	99.72	99.86	99.78
Physical Activity	99.86	99.86	99.86
Cognitive Stress	99.59	99.86	99.72
Emotional Stress	100.00	99.59	99.79
	Accuracy	**99.61**%	

CNN have almost the same results, while due to having less trainable parameters, 1D CNN is significantly faster than 2D CNN., hence it can be a better choice in this case.

Table 5. Comparing CNN with SVM and RF

Classifier	Accuracy (%)	F1-Score (%)
SVM	84.45	84.25
RF	92.29	92.50
1D CNN	**99.82**	99.78
2D CNN	99.61	99.77

4.4 Adding Noise

In order to challenge our proposed approach, we added a white noise with zero mean and standard deviation 1 to all the sequences and trained all previously mentioned models again. Table 6 shows the performance of all methods resulted after training with the noisy dataset. It is observable that CNN models significantly outperforms SVM and RF in presence of noise. However, it should be noticed that in this case, 2D CNN outperforms 1D CNN which is because of having 2D kernels, i.e., 2D CNN has more trainable parameters and can learn more detailed features from the dataset, hence it can be more powerful than 1D CNN in complex problems.

Table 6. Comparison results after adding noise to the dataset

Classifier	Accuracy	F1-Score (%)
SVM	70.25	65.75
RF	71.84	69.23
1D CNN	93.54	93.47
2D CNN	**97.46**	**97.32**

5. SUMMARY AND CONCLUSION

In this paper we exploited deep learning approach to solve classification problems in a multi-modal physiological time series dataset recorded from wrist-worn sensors. After some preprocessing steps, we obtained 99.82% and 99.61% classification accuracy as well as 99.78% and 99.77% F1-score for 1D and 2D CNN models, respectively. As for the comparison, we trained two well-known machine learning algorithms in classification problems, multi-class SVM and RF, using our manually extracted features. The results prove that both 1D and 2D CNN models outperform SVM and RF method, however, due to being computationally more affordable, 1D CNN algorithm is faster than 2D CNN. Moreover, to make it more challenging, we added a white noise with zero mean and variance 1 to the dataset and trained all the models again. This time also, both CNN models outperformed SVM and RF, even more significantly, while due to having 2D convolution kernels and consequently more trainable parameters, 2D CNN performed better than 1D CNN. Hence we showed that

the robustness to noise characteristics of the CNN models in comparison to the machine learning algorithms, makes them very useful tools in working with noisy datasets, like physiological time series or medical datasets. Moreover, we could see that CNN models generate features general enough to show promising performance on previously unseen test dataset.

Our future work will be devoted to leveraging these methodology on more challenging physiological datasets, and also using this methodology for other purposes like designing a predictive or prohibiting device, informing the patients prior to having high levels of stress which may put them into unpleasant health conditions.

REFERENCES

Al-Shargie, F., Tang, T.B., Badruddin, N., and Kiguchi, M. (2015). Mental stress quantification using eeg signals. In *International Conference for Innovation in Biomedical Engineering and Life Sciences*, 15–19. Springer.

Chaovalitwongse, W.A., Fan, Y.J., and Sachdeo, R.C. (2007). On the time series k-nearest neighbor classification of abnormal brain activity. *IEEE Transactions on Systems, Man, and Cybernetics-Part A: Systems and Humans*, 37(6), 1005–1016.

Chen, L. and Ng, R. (2004). On the marriage of lp-norms and edit distance. In *Proceedings of the Thirtieth international conference on Very large data bases-Volume 30*, 792–803.

Choudhary, D., Jaloli, M., and Cescon, M. (2020). Characterising sympathetic response with power spectral density analysis.

Cogan, D., Pouyan, M.B., Nourani, M., and Harvey, J. (2014). A wrist-worn biosensor system for assessment of neurological status. In *2014 36th Annual International Conference of the IEEE Engineering in Medicine and Biology Society*, 5748–5751. IEEE.

Deng, H., Runger, G., Tuv, E., and Vladimir, M. (2013). A time series forest for classification and feature extraction. *Information Sciences*, 239, 142–153.

Dopfel, D. and Zhang, N. (2018). Mapping stress networks using functional magnetic resonance imaging in awake animals. *Neurobiology of stress*, 9, 251–263.

Ebadi, N., Lwowski, B., Jaloli, M., and Rad, P. (2019). Implicit life event discovery from call transcripts using temporal input transformation network. *IEEE Access*, 7, 172178–172189.

Farrell, S.P., Hains, A.A., Davies, W.H., Smith, P., and Parton, E. (2004). The impact of cognitive distortions, stress, and adherence on metabolic control in youths with type 1 diabetes. *Journal of Adolescent Health*, 34(6), 461–467.

Ghiasi, S., Greco, A., Barbieri, R., Scilingo, E.P., and Valenza, G. (2020). Assessing autonomic function from electrodermal activity and heart rate variability during cold-pressor test and emotional challenge. *Scientific Reports*, 10(1), 1–13.

Goldberger, A.L., Amaral, L.A., Glass, L., Hausdorff, J.M., Ivanov, P.C., Mark, R.G., Mietus, J.E., Moody, G.B., Peng, C.K., and Stanley, H.E. (2000). Physiobank, physiotoolkit, and physionet: components of a new research resource for complex physiologic signals. *circulation*, 101(23), e215–e220.

Greco, A., Valenza, G., Lanata, A., Scilingo, E.P., and Citi, L. (2015). cvxeda: A convex optimization approach to electrodermal activity processing. *IEEE Transactions on Biomedical Engineering*, 63(4), 797–804.

He, K., Zhang, X., Ren, S., and Sun, J. (2015). Delving deep into rectifiers: Surpassing human-level performance on imagenet classification. In *Proceedings of the IEEE international conference on computer vision*, 1026–1034.

Islam, R., Lee, Y., Jaloli, M., Muhammad, I., Zhu, D., and Quarles, J. (2020). Automatic detection of cybersickness from physiological signal in a virtual roller coaster simulation. In *2020 IEEE Conference on Virtual Reality and 3D User Interfaces Abstracts and Workshops (VRW)*, 649–650. IEEE.

Ji, S., Xu, W., Yang, M., and Yu, K. (2012). 3d convolutional neural networks for human action recognition. *IEEE transactions on pattern analysis and machine intelligence*, 35(1), 221–231.

Kampouraki, A., Manis, G., and Nikou, C. (2008). Heartbeat time series classification with support vector machines. *IEEE Transactions on Information Technology in Biomedicine*, 13(4), 512–518.

Karpathy, A., Toderici, G., Shetty, S., Leung, T., Sukthankar, R., and Fei-Fei, L. (2014). Large-scale video classification with convolutional neural networks. In *The IEEE Conference on Computer Vision and Pattern Recognition (CVPR)*.

Kellaway, F. (1969). Advanced engineering mathematics. byerwin kreyszig. pp. xx, 899. 68s.(wiley.). *The Mathematical Gazette*, 53(386), 444–444.

Keogh, E. and Kasetty, S. (2003). On the need for time series data mining benchmarks: a survey and empirical demonstration. *Data Mining and knowledge discovery*, 7(4), 349–371.

LeCun, Y., Bengio, Y., and Hinton, G. (2015a). Deep learning. *nature*, 521(7553), 436–444.

LeCun, Y. et al. (2015b). Lenet-5, convolutional neural networks. *URL: http://yann. lecun. com/exdb/lenet*, 20(5), 14.

Liu, C., Zhou, Q., Li, Y., Garner, L.V., Watkins, S.P., Carter, L.J., Smoot, J., Gregg, A.C., Daniels, A.D., Jervey, S., et al. (2020). Research and development on therapeutic agents and vaccines for covid-19 and related human coronavirus diseases.

Mueller, S.M., Heistad, D.D., and Marcus, M.L. (1979). Effect of sympathetic nerves on cerebral vessels during seizures. *American Journal of Physiology-Heart and Circulatory Physiology*, 237(2), H178–H184.

Posada-Quintero, H.F., Reljin, N., Mills, C., Mills, I., Florian, J.P., VanHeest, J.L., and Chon, K.H. (2018). Time-varying analysis of electrodermal activity during exercise. *PloS one*, 13(6), e0198328.

Rajpurkar, P., Hannun, A.Y., Haghpanahi, M., Bourn, C., and Ng, A.Y. (2017). Cardiologist-level arrhythmia detection with convolutional neural networks. *arXiv preprint arXiv:1707.01836*.

Ratanamahatana, C.A. and Keogh, E. (2005). Three myths about dynamic time warping data mining. In *Proceedings of the 2005 SIAM International Conference on Data Mining*, 506–510. SIAM.

Zeiler, M.D. and Fergus, R. (2014). Visualizing and understanding convolutional networks. In *European conference on computer vision*, 818–833. Springer.